RESEARCH ARTICLE

Salt leaching as a green method for the production of polyethylene foams for thermal energy storage applications

Alessandro Sorze [ID] | Francesco Valentini [ID] | Andrea Dorigato |
Alessandro Pegoretti

Department of Industrial Engineering and INSTM Research Unit, University of Trento, Trento, Italy

Correspondence
Alessandro Sorze and Alessandro Pegoretti, Department of Industrial Engineering and INSTM Research Unit, University of Trento, Via Sommarive 9, 38123 Trento, Italy.
Email: alessandro.sorze@unitn.it and alessandro.pegoretti@unitn.it

Abstract

Materials able to store thermal energy can be a useful strategy to reduce energy consumption of buildings and to decrease greenhouse gases emissions. In this work, for the first time, the technique of salt leaching has been used to produce novel polyethylene foams containing different amounts of a microencapsulated phase-change material (PCM) with a melting point of 24°C, to be potentially applied in building insulation. The microstructural, thermal, and mechanical properties of produced foams have been comprehensively investigated. The prepared foams were characterized by high values of open porosity (about 60%) and by density values around 0.4 g/cm^3. Infrared thermography analysis demonstrated that the time required from the samples to reach a set temperature, thanks to the presence of PCM, was up to two times higher with respect to the reference foam. Therefore, these materials could store/release an interesting amount of thermal energy. Shore-A measurements evidenced that the addition of PCM generally led to a softening of the foams. Tensile mechanical tests confirmed the softening effect provided by the addition of the microcapsules, with a decrease of the stiffness and of the strength of the material. Interestingly, strain-at-break values were considerably increased upon PCM introduction.

KEYWORDS
foams, phase-change materials, polyethylene, salt leaching, thermal energy storage

1 | INTRODUCTION

Recently, the improved living conditions of people and the increase of growth rate of population have led to an enhancement of the energy demands for buildings. Recent studies have found that the primary source of energy in the world will continue to be fossil fuels up to 2030.[1] The development of sustainable buildings and renewable energy resources is thus becoming an important issue for our society. In fact, the building sector is one of the most energy consuming, with an overall energy consumption of 30% in the world[1] (40% in Europe[2]) and it is responsible for one-third of the world-wide emissions of greenhouse gases.[3] Taking in consideration that the energy needs for hot water and heating is lower than the annual solar energy incident on buildings, the possibility of a thermal management of renewable energy is a crucial point both in building and automotive sectors in order to minimize energy consumption and toxic gases emissions.[4,5] The ability of a material to temporarily store heat and release it in a second time is a process called thermal energy storage (TES).[4,6,7] Latent

heat TES systems are particularly promising, because of their capacity to store heat at constant temperature upon a phase change in the material. Phase-change materials (PCMs) are thus designed for the storage of a considerable amount of heat when they undergo a reversible solid-to-liquid transition at a constant temperature.[8–12] Examples of PCMs are paraffin waxes,[13–16] fatty acids,[17] polyethylene glycol (PEG),[18] fatty alcohols,[19] salt hydrates, and metals.[12,20] Paraffins are organic PCMs and they are widely employed for thermoregulation of buildings,[10,21] sportswear[22] and smart fabrics,[23–25] thanks to their low cost, high heat of fusion, cheapness, noncorrosive behavior, chemically inertness, thermal stability, little volume changes on melting, and low vapor pressure in the molten state.[8,9,26,27] PCMs can be encapsulated in order to avoid leakage above the melting temperature, increasing thus their strength, durability and thermal stability, and easy-handling and reliability.[25,28,29] A second strategy to avoid PCM leakage is the shape stabilization[15,30,31]: it consists in the confinement of the PCM within a polymer matrix, such as high-density polyethylene,[32] polypropylene,[33] poly(methylmethacrylate),[34] polyurethane copolymers,[35] acrylic resins,[36] styrene–butadiene–styrene rubber, and ethylene-propylene-diene-monomer (EPDM) rubber.[13] The integration of PCM inside buildings can improve the management of indoor temperature reducing the cooling costs in the hot season. Lee et al. demonstrated that PCM-enhanced cellulose insulation in residential building walls led to a reduction of daily average peak heat flux of about 20%.[37] Hanchi et al. showed that the insertion of PCM in roofs can lead to a reduction of energy consumptions.[38] Wang et al. evaluated the thermal performances of honeycomb wallboard combined with mPCM,[39] highlighting that the heat can be efficiently dissipated in different indoor environment conditions.

Polymeric foams are expanded materials in which the porosity is obtained using chemical or physical blowing agents. In comparison with bulk polymers, they present low density, low thermal conductivity, high insulation capacity, elevated thermal stability, and also good mechanical properties in terms of toughness and impact resistance.[40] In recent years, polyolefins have found wide interest as matrices for the foaming process. In fact, polyolefin foams are characterized by a wide range of properties that allow them to be employed as insulation materials in various fields such as buildings, automotive, military, aerospace, aircraft, sports, and so on.[41,42] Polyethylene foams are generally used for the production of gaskets and vibration pads, sound insulation, water barriers, expansion joints, pipe insulation, and glazing seals. They are used in a wide range of density from 0.15 to 0.60 g/cm^3.[43] Physical blowing agents are inert gases,

which are introduced into the polymer matrix during a saturation process, usually at high pressure.[40] The most widely used physical blowing agents are nitrogen (N_2), carbon dioxide (CO_2) or hydrocarbons such as pentane. Chemical blowing agents are powders that can induce an exothermic or endothermic reaction inside the polymer matrix through their thermal decomposition, generating thus a gas phase. The most common one is azodicarbonamide (ADC) which decomposes at around 170–200°C and possesses high gas yield, releasing nitrogen and heat.[41,44–46] Examples of endothermic chemical blowing agents are sodium bicarbonate and zinc bicarbonate.[47] Although chemical blowing agents are widely used, many of them are forbidden by the European Union since they are hazardous to health.[46] Therefore, water, hydrocarbons, or other more available physical foaming agents are often required.[48,49] However, physical blowing agents generally show some problems related to the difficult manufacturing process and the use of additional and expensive equipment.[46]

One possible technique for the foam production that seems to overcome all the problems related to the use of traditional chemical and physical blowing agents is represented by the "salt leaching" technology. This eco-friendly method provides the production of materials with porous cellular structure by mixing the polymer matrix with water-soluble salt particles, like sodium chloride or potassium chloride. Then, placing the sample in hot water the salt particles dissolve, forming the final foam morphology.[50–53] This method has been widely applied for the preparation of scaffolds,[51,52,54] plastic semiconductors,[55] open cell nitrile–butadiene–rubber (NBR) sponges,[56] EPDM foams,[57,58] applied in tissue engineering and for soft sensors.[59] By tuning the polymer-to-salt ratio and by varying the leachable particle size, the porosity of the resulting scaffolds may range between 70% and 95%. Moreover, salt leaching maybe used in combination with other techniques (gas foaming, compression molding) in order to further modify the structure of the foams, increasing the pore interconnectivity.[60]

Although the environmental advantages that could arise from the combination of polyethylene foams produced through particle leaching and the TES capability through the addition of PCM within the polymeric matrix, no studies can be found in the open literature on this topic. This work is thus focused on the development of polyethylene foams produced through salt leaching technique and containing different amounts of a microencapsulated PCM with a melting point of 24°C. The resulting materials could be potentially employed for the thermal management in the building sector and as thermo-acoustic insulators for thermal plants. The microstructural behavior of the prepared foams was correlated with their thermal and mechanical properties.

2 | EXPERIMENTAL

2.1 | Materials

High-density polyethylene (HDPE) ELTEX A4040P (density = 0.94 g/cm^3, melt flow index [MFI] at 190°C/2.16 kg = 3.5 g/10 min) was purchased from Ineos polyolefins (Rolle, Switzerland) in form of fine powder. Poly-ethyleneglycol (PEG) in form of granules, with a molecular weight of 2000 Da, was provided by Alfa Aesar (Kandel, Germany) and used to improve the leaching efficiency. Sodium chloride, commercial grade (density = 2.16 g/cm^3), was grinded and sieved using a 230-mesh sieve in a gran-ulometry lower than 63 μm. Preliminary tests were carried out in order to determine the granulometry value that allowed to minimize the density of the foam, and a salt size lower than 63 μm was thus selected. Before the use, the selected salt was placed in an oven at 60°C to be dried. MPCM24 microcapsules containing a wax with a melting point of 24°C and a melting enthalpy of 145 J/g were pur-chased from Microtek Laboratories Inc. (Dayton, OH, USA) and used as PCM. In Table 1, the main features of MPCM24 are reported. Polyethylene powder, PEG, and microcapsules were used as received.

2.2 | Samples preparation

The production of polyethylene foams was carried out by using an internal mixer (Thermo Haake Rheomix® 600), provided of counter rotating rotors. The compounding process was performed at a temperature of 153°C and a rotor speed of 50 rpm. The polymer matrix and the PCM were manually mixed and then added to the melt com-pounder, where they were mixed for 5 min. Salt and poly-ethylene glycol were then gradually added into the mixer. The average mixing procedure time was about 20 min for each sample. The resulting compounds were then

TABLE 1 Properties of paraffin microcapsules utilized in this work

Properties	Specification (value)
Appearance	White to slightly off-white color
Capsules composition	85–90 wt% PCM 10–15 wt% polymer shell
Core material	Paraffin
Particle size	14–24 μm
Melting temperature	24°C
Heat of fusion	145–155 (J/g)
Specific gravity	0.9 g/cm^3

compression molded at a temperature of 180°C for 13 min. The pressure was set at 1 bar for the first 3 min and at 7 bar and for the next 10 min. In this way, square sheets of polyethylene (dimensions of 100 × 100 × 2 mm^3) with different PCM amounts were obtained. The leaching method described by Scaffaro et al.[52] was taken as a reference for the present work. Pressed samples were thus immersed in boiling demineralized water for 3 h in order to obtain a proper salt dissolution. The obtained foams where then dried overnight in an oven at 60°C.

The list of the samples with their codes is reported in Table 2. Their designation is formed by the term PE followed by the average size of the salt particles (<63 μm) used for the foams production and by the PCM content expressed in phr (per hundred resin).

2.3 | Experimental methodologies

2.3.1 | Preliminary tests

Residual salt and water uptake measurements
The quantity of residual salt (RS) not dissolved during the leaching process has been calculated according to Equation (1):

$$RS = \frac{m_{dry} - m_{tot}}{m_{dry}}, \quad (1)$$

where m_{dry} is the mass of the final foam after the leaching technique and its subsequent drying and m_{tot} is the ideal mass of the final foam in case of complete disso-lution, evaluated according to Equation (2):

$$m_{tot} = m_0 - m_{NaCl} - m_{PEG} \quad (2)$$

where m_0 is the mass of the sample before salt leaching, m_{NaCl} is the initial mass of the salt in the blend (30 g), and m_{PEG} is the initial mass of the PEG in the blend (2 g). A foam connectivity parameter (C) has been evalu-ated in order to study the continuity of the pores and also the dissolution of the foaming agents (PEG, NaCl), according to Equation (3)[52]:

$$C = \frac{(m_0 - m_{dry})}{m_{NaCl} + m_{PEG}} \quad (3)$$

Water uptake analyses were performed in order to study the water absorption tendency of the foams that were related to their porosity. These tests were carried out according to the methodology reported in the ASTM D570 standard: samples were previously dried for 24 h in

TABLE 2 List of the prepared samples

Sample	HDPE (g)	NaCl (phr)	PEG (phr)	PCM (phr)	PCM (wt%)
PE_ < 63s	8	375	25	0	0
PE_ < 63s_25_p	8	375	25	25	20.0
PE_ < 63s_50_p	8	375	25	50	33.3
PE_ < 63s_100_p	8	375	25	100	50.0
PE_ < 63s_130_p	8	375	25	130	56.5

Abbreviations: HDPE, high-density polyethylene; PEG, polyethyleneglycol; PCM, phase-change material.

oven at 50°C and then weighted, they were then immersed in demineralized water for a certain amount of time, and then weighted again. The mass of the samples was measured with a Kern KB3600 balance (10 mg sensitivity). The mass measurements of every specimen were carried out after immersion in water for 30 min, 1 h, 2 h, 8 h, and 24 h. The water uptake (WU) has been calculated according to Equation (4):

$$WU = \frac{m_{wet} - m_{dry}}{m_{dry}} \quad (4)$$

where m_{wet} is the mass of the sample after the immersion in water and m_{dry} is the sample mass after drying.

Leaking tests

The ability of the foams to avoid paraffin leakage was evaluated performing 50 heating/cooling cycles between temperatures of 0 and 40°C by using an Angelantoni climatic chamber. Each cycle lasted 3 h and the specimens were placed on a paper towel in order to absorb an eventual paraffin leakage. The weight was taken before and after the test, and the mass loss was evaluated.

2.3.2 | Morphological properties

Micrographs of the foams were obtained by using a field emission scanning electron microscope (FESEM) AG-Supra 40, operating at an accelerating voltage of 2.5 kV inside a chamber under a vacuum of 10^{-6} Torr. Before the observations, the samples were cryofractured and then a deposition of a thin electrically conductive Pt/Pd coating has been conducted. From SEM micrographs, the pore-size distribution of the foams has been evaluated through the use of software ImageJ.

Helium pycnometry density (ρ_{picn}) tests were performed using a gas displacement AccuPycII 1330 pycnometer at a temperature of 23°C. For every specimen, 30 replicate measures were carried out. The geometrical density (ρ_{geom}), representing the value of the mass over the total volume (including solid, open, and closed

porosity), was measured on five cylindrical specimens (18 mm in diameter), by weighing them with a Gibertini E42 balance (resolution of 0.1 mg) and their dimensions using a digital caliper with a resolution of 0.01 mm.

Residual salt was taken into account for the density measurements; therefore, mixture rule (Equation 5) has been used.

$$\rho_F = \frac{W_F}{\frac{1}{\rho_c} - \frac{W_{RS}}{\rho_{RS}}} \quad (5)$$

where ρ_F is the effective density of the foam considering the residual salt content, ρ_c is the geometric density of the foam (containing residual salt), W_{RS} and W_F are the weight fraction of residual salt and expanded material (without residual salt), respectively, and ρ_{RS} is the density of salt (2.16 g/cm³).[61] According to ASTM D6226 standard, it was possible to calculate the total porosity (P_{tot}) and the fraction of open porosity (OP) and closed porosity (CP) according to Equations (6)–(8):

$$P_{tot} = 1 - \frac{\rho_{geom}}{\rho_{bulk}} \quad (6)$$

$$OP = 1 - \frac{\rho_{geom}}{\rho_{picn}} \quad (7)$$

$$CP = P_{tot} - OP \quad (8)$$

where ρ_{bulk} is the density of the nonexpanded polymer matrix (equal to 0.914 g/cm³) obtained from pycnometric measurements.

2.3.3 | Thermal properties

The thermal degradation behavior of the produced samples was investigated through thermogravimetric analysis (TGA) using a Mettler TG50 thermobalance under a heating ramp from 30 to 700°C, at rate of 10°C/min in a nitrogen environment of 10 ml/min. The temperature at

which there is the 5% of mass loss of ($T_{5\%}$), the temperatures of maximum rates of mass loss of the PCM and of the PE matrix (respectively denoted as T_{peak1}, T_{peak2}) and the residual mass at 400°C (m_{400}) were determined.

Differential scanning calorimetry (DSC) measurements were performed on the prepared samples using a Mettler DSC30 calorimeter under a nitrogen flow of 100 ml/min. A first heating scan from −30 to 70°C was followed by a cooling stage from 70 to −30°C and by a second heating scan from −30 to 70°C. All the thermal ramps were carried out at 10°C/min. In this way, it was possible to determine the most important thermal properties of the PCM: specific melting and the crystallization enthalpy values (ΔH_{m1}, ΔH_c, ΔH_{m2}), melting temperature during the first and the second heating scan (T_{m1}, T_{m2}) and crystallization temperature (T_c). Moreover, the study of the effective PCM content in the foams during the first heating scan (PCM_{m1}^{eff}), the cooling scan (PCM_c^{eff}), and the second heating scan (PCM_{m2}^{eff}) was performed considering the ratio between the specific enthalpy of the samples and the corresponding specific enthalpy values of the neat PCM, as shown in Equations (9)–(11):

$$PCM_{m1}^{eff} = \frac{\Delta H_{m1}}{\Delta H_{m1PCM}} \qquad (9)$$

$$PCM_c^{eff} = \frac{\Delta H_c}{\Delta H_{cPCM}} \qquad (10)$$

$$PCM_{m2}^{eff} = \frac{\Delta H_{m2}}{\Delta H_{m2PCM}} \qquad (11)$$

where ΔH_{m1PCM}, ΔH_{cPCM}, and ΔH_{m2PCM} are the specific phase-change enthalpy values of the neat PCM collected during first heating scan, cooling, and second heating scan, respectively.

The TES efficiency of the produced foams was studied monitoring the evolution of the surface temperature of the samples during heating/cooling cycles, using an infrared thermal camera FLIR E60 (emissivity = 0.86). The samples were heated in an oven at 40°C overnight and then placed in a climatic chamber at a temperature of 5°C, and their surface temperature was then monitored until the thermal equilibrium between the samples and the environment was reached. In the same way, the specimens were cooled in a refrigerator at 0°C overnight and then inserted in an oven at a temperature of 40°C. In the heating tests, the time required to reach a temperature of 40°C (t_{40}) has been evaluated and in the cooling tests, the time required to reach a temperature of 5°C (t_5) has been determined.

Thermal conductivity tests were performed following ISO 22007 standard on squared specimens with dimensions of $20 \times 20 \times 2$ mm³, using a Hot Disk thermal analyzer provided of a sensor having a diameter of around 2.0 mm. The analysis was carried out at a temperature of 22°C, applying a power of 20 mW for 5 s in case of foamed materials. The choice of these operating parameters was performed to ensure an increase of the temperature of at least 2°C for each specimen, as reported in the standard. At least three measurements were performed for each sample.

2.3.4 | Mechanical properties

Shore A hardness test was performed using a Hilderbrand Prufstander OS2 durometer following the ASTM D2240 standard. Square samples 20 mm wide and 2 mm thick were tested, and Shore A hardness was evaluated after a loading time of 5 s. At least five measurements were performed for each composition.

Tensile properties of the prepared foams under quasi-static conditions were measured on ISO 527 type 1BA dumbbell specimens (gauge length equal to 30 mm) using an Instron 5969 tensile testing machine equipped with a load cell of 100 N and operating at a cross-head speed of 1 mm/min. The elastic modulus (E) has been calculated as a secant modulus between strain values of 0.0005 mm/mm and 0.0025 mm/mm. The stress at break (σ_R) and the strain at break (ε_R) have been also evaluated. At least five specimens were tested for each composition. Both the elastic modulus and the stress at break values were normalized for the geometrical density of the foams.
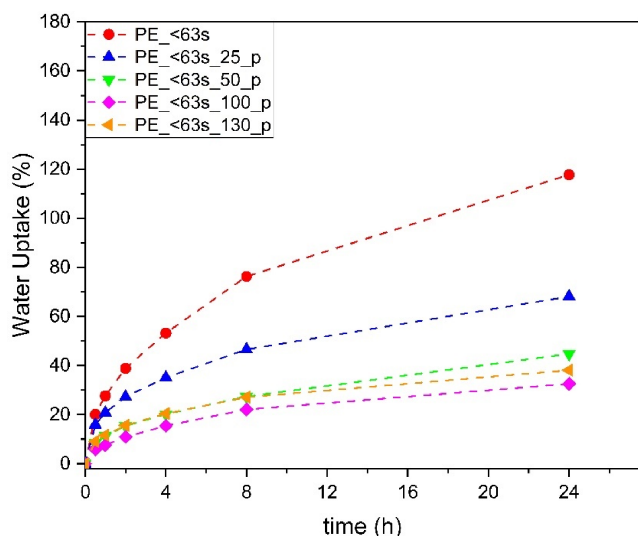
3 | RESULTS AND DISCUSSION

3.1 | Preliminary tests

3.1.1 | Residual salt and water uptake measurements

Table 3 displays the residual salt and the connectivity values obtained for the prepared foams, evaluated according to Equations (1)–(3). It is possible to observe that the percentage of residual salt does not depend on the PCM content and it is around 10%–13% for all the samples, except for PE_ < 63s_100_p foam that is characterized by a higher residual salt content (around 27 wt%), probably because of an inhomogeneous salt dispersion during the production stage. However, the connectivity decreases as the content of PCM inside the foam increases, passing from 80% for the neat PE foam up to 47% for the PE_ < 63s_130_p sample. This could be

TABLE 3 Residual salt and connectivity values obtained for the prepared foams

Sample	Residual salt (wt%)	Connectivity (%)
PE_ < 63s	10.8	80.0
PE_ < 63s_25_p	10.8	71.0
PE_ < 63s_50_p	12.4	65.7
PE_ < 63s_100_p	27.3	47.6
PE_ < 63s_130_p	13.3	47.3

TABLE 4 Results of the leaking tests

Sample	Mass loss (wt%)
PE_ < 63s_25_p	1.65
PE_ < 63s_50_p	0.83
PE_ < 63s_100_p	0.84
PE_ < 63s_130_p	1.49

FIGURE 1 Results of the water uptake measurements on the prepared foams

explained by the fact that the PCM filled some of the pores, thus limiting the interconnections among them.

In Figure 1, the water uptake values, calculated according to Equation (4), are reported as function of the testing time. The parabolic shape of the curves indicates that the water absorption in these foams is mainly governed by a diffusion mechanism[62] and that the absorption rate decreases with time, reaching in some cases a plateau after 24 h. It is interesting to notice that increasing the PCM amount inside the foams, the water uptake decreases. This could suggest that the addition of more PCM leads to a decrease in the porosity and thus, in the volume available for water absorption. This feature can be also correlated to the decrease of the connectivity observed in Table 3. In fact, the increase of the PCM content in the foams leads to the formation of a less interconnected structure and thus to a lower water absorption capability.

3.1.2 | Leaking tests

Table 4 shows the values of the mass loss after 50 heating/cooling cycles. For all the sample the mass

loss is almost negligible, meaning that these materials work efficiently also after many thermal cycles.

3.2 | Morphological properties

The morphological features of the foamed samples were studied through scanning electron microscopy (SEM) observations. In Figure 2A–F, representative SEM micrographs at 500× and 5000× of the foamed samples are reported. It is possible to observe that the prepared foams are characterized by an open porosity with pores dimension, in the case of the PE_ < 63s, of 21.4 ± 14.7 μm, that decreases upon PCM addition reaching a value of 10.1 ± 4.1 μm for the PE_ < 63s_130_p foam. Moreover, from Figure 2D, a poor adhesion between paraffin microcapsules and the PE matrix, together with an evident interfacial debonding, can be observed. It has to be considered that the PCM is contained in a melamine-formaldehyde shell, probably characterized by a limited chemical compatibility with polyolefin matrices. In general, few capsules can be detected in these micrographs, meaning that PCM distribution is not homogeneous in the foams but also that part of PCM could have been lost during the melt compounding and the subsequent leaching process. However, the morphology of the prepared foams is quite similar to that of PLA scaffolds produced by Scaffaro et al. through the salt leaching method using a salt grain size of 45–65 μm.[52] In both cases, indeed, the materials are characterized by an elevated degree of interconnected pores, with very thin cell walls. The addition of PCM in the foams leads to a less porous structure, since paraffin capsules are bulk materials that occupy some of the pores (see Figure 2E). Moreover, the addition of PCM results in an increase of the residual salt concentration, clearly visible in Figure 2F in form of cubic particles. These residues did not dissolve during salt leaching, because they are too small (about 4.5 μm) and also because PCM particles could have hindered in some way the complete leaching of salt granules.

In Figure 3, the pore-size distribution of the prepared foams is reported.

From Figure 3, it can be observed that the pore-size distribution is independent from the amount of PCM that
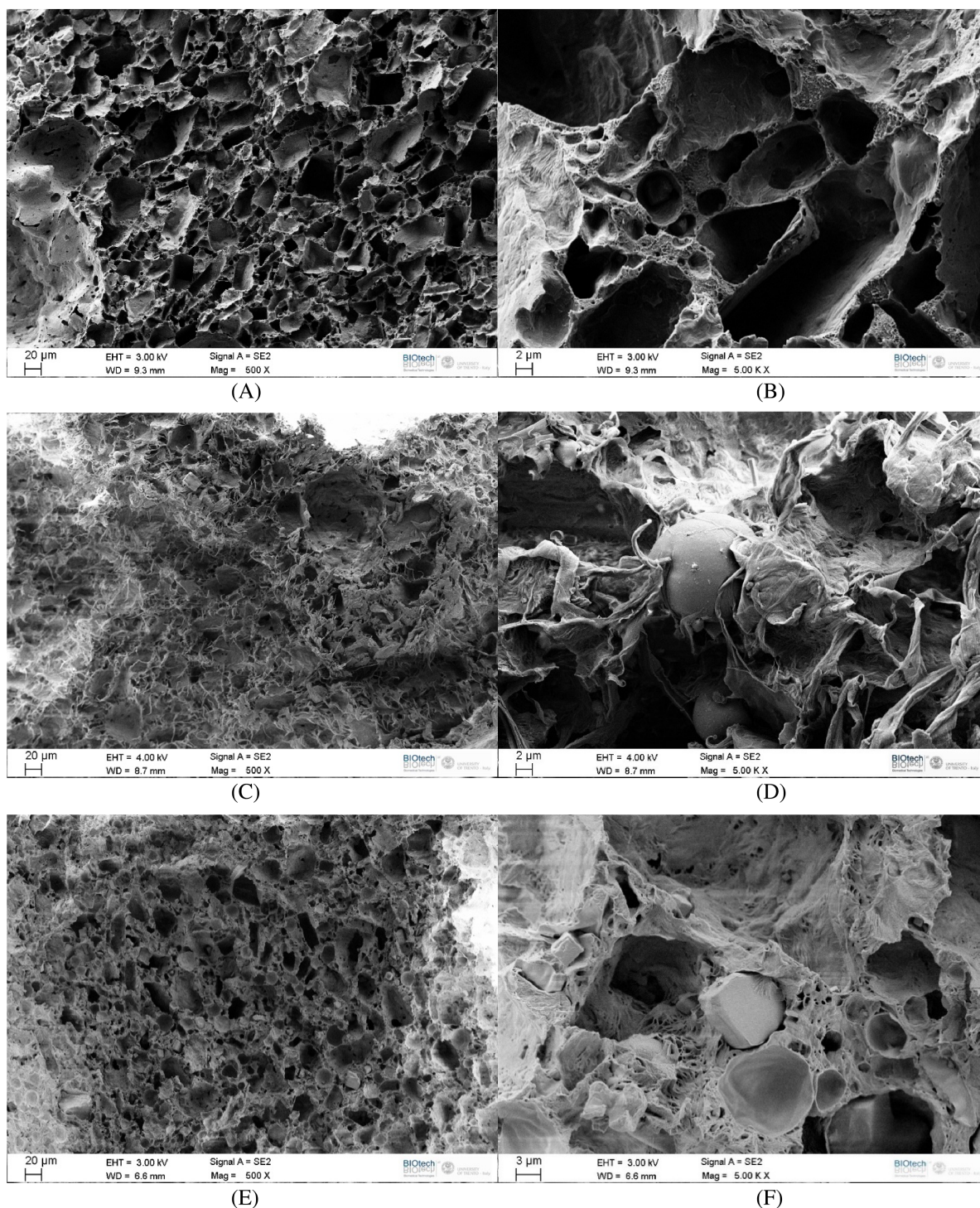
FIGURE 2   SEM micrographs of the prepared foams: (A) PE_ < 63s, 500x; (B) PE_ < 63s, 5000 x; (C) PE_ < 63s_50p, 500x; (D) PE_ < 63s_50p, 5000x, (E) PE_ < 63s_130p, 500x; (F) PE_ < 63s_130p, 5000x

it is added to the foams, and the average pore size is around 5–7 μm for all the samples, except for the PE_ < 63s_100_p foam. PE_ < 63s_100_p shows a larger pore-size distribution, and this can be related to nonoptimal mixing of the starting materials during sample preparation, that led to inhomogeneities in the structure of this foam. It should be also noted that the pore-size dimension is coherent with the

salt size used for the leaching process, since it was selected as lower than 63 μm and therefore comprehensive of very low particles in the range of 5–7 μm.

From the results of density measurements, shown in Table 5, it is possible to notice the geometrical density increases with the PCM amount, since the microencapsulated paraffin remains in the foam after salt leaching

technique filling some of the pores. On the other hand, the pycnometric density values are practically unaffected by the content of PCM in the foams and are systematically higher than the corresponding geometric density values. This could be explained by the fact that, with the salt leaching method, the produced foams have an elevated degree of interconnection of the pores (see Table 3) and an open pores structure (see Figure 2). In these conditions, the density values obtained through pycnometric measurements are close to bulk density of PE (taking also into account the PCM content and the residual salt concentration).

Table 5 also shows the total and open porosity values of the foams as a function of PCM content, evaluated according to Equations (6) and (7). It is possible to notice that increasing the PCM content, the porosity values decrease, since PCM microcapsules occupy some of the pores. For example, comparing PE_ < 63s and PE_ < 63s_130_p foams, the total porosity decreases from 65% to 45% upon the PCM addition. On the other hand, the total and the open porosity values for every sample are quite similar, meaning that the closed porosity is practically negligible in all the produced samples. This effect was also observed in a previous work where the salt

leaching technique was used for the production of EPDM rubber foams.[57]

3.3 | Thermal properties

Thermogravimetric curves and corresponding derivative plots of prepared foams, are represented in Figure 4A,B and the most significative results are listed in Table 6. From curves of PE_ < 63s samples, it is evident that the foaming stage produces a slight decrease of the thermal stability of the samples, with a shift of thermogravimetric curves toward lower temperatures respect to the theoretical values characteristic of a bulk PE. This behavior can be explained considering the increased surface area exposed to degradation in the case of foams, the presence of preferential pathways for release of by-products due to the presence of an open porosity and the oxidative processes due to the air entrapped in the pores.[57,63] From Figure 4A a first degradation stage, between 200°C and 400°C, can be seen only in the foamed samples with PCM, and this is associated with PCM degradation (T_{peak1}), while a second degradation stage, corresponding to the degradation of the PE matrix occurs at about 485°C (T_{peak2}). From the results reported in Table 6, it is evident that both T_{peak1} and T_{peak2} are not substantially affected by the PCM content in the foams. As it could be expected, the thermal degradation stability of the foams is negatively influenced by the PCM addition. As it can be seen in Table 6, the values of $T_{5\%}$ decrease as the content of PCM increases (from 398°C in the case of PE_ < 63s sample to 185°C for the PE_ < 63s_130_p foam). It should be considered that the set temperature values are much higher than those reached in an eventual application in buildings of these foams, and the observed drop of the thermal stability should not dramatically limit their technical employability of the prepared foams in this field.

It is also possible to check whether the mass loss values between 200 and 400°C are coherent with the PCM content in the foams. From the m_{400} values detected for PE_ < 63s_25_p, PE_ < 63s_50_p, and PE_ < 63s_100_p
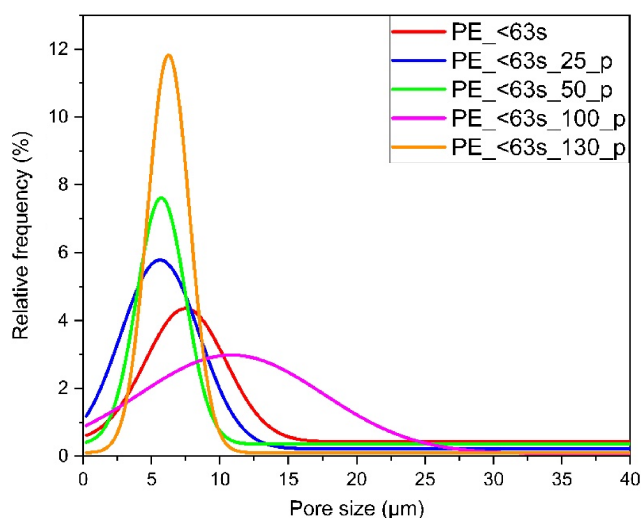

FIGURE 3 Pore-size distribution of the prepared foams

TABLE 5 Density results for the prepared foams

Sample	Geometric density (g/cm^{-3})	Pycnometric density (g/cm^{-3})	Total porosity (%)	Open porosity (%)
PE_ < 63s	0.32 ± 0.01	8.7 ± 0.8	63.7 ± 2.9	65.9 ± 2.8
PE_ < 63s_25_p	0.37 ± 0.05	0.84 ± 0.05	59.8 ± 5.5	56.4 ± 5.9
PE_ < 63s_50_p	0.45 ± 0.08	0.87 ± 0.04	50.0 ± 9.1	47.6 ± 9.5
PE_ < 63s_100_p	0.43 ± 0.11	1.00 ± 0.03	53.4 ± 12.1	57.6 ± 11.0
PE_ < 63s_130_p	0.52 ± 0.07	0.90 ± 0.02	43.1 ± 8.3	42.5 ± 8.3

foams, it is possible to conclude that the PCM content within the foams is, respectively, 10.4%, 22.7%, and 40.6%. These values are comparable with the PCM contents reported in Table 2 and recalculated considering the residual salt content in each sample (i.e., 16.0%, 28.9%, and 37.4%, respectively). In the case of PE_ < 63s_100_p foam, the mass loss value is slightly higher than the nominal PCM content and this result can be explained by an

inhomogeneous distribution of PCM inside the sample. For the PE_ < 63s_130_p foam, the PCM content is 35.3%, much lower than the expected one (i.e., 49.0%, value of Table 2 re-calculated considering the residual salt content in the sample), meaning that some PCM could have been lost during the compounding operations and the subsequent leaching process.

DSC curves of the prepared foams and of neat PCM are showed in Figure 5A–C and the most relevant results are summarized in Table 7. In Figure 5A,C, the first and second heating scans are reported and in both figures two endothermic peaks can be observed. The first peak, approximately at 20–25°C, is associated with the melting of paraffin and its intensity increases with the PCM content in the foams. The second peak, observed at around 50°C, is associated with the melting of PEG that remained in the foam and has not been fully dissolved.

In Figure 5B, the thermograms referred to the cooling scan are represented. In this case a double exothermic peak in the temperature interval from -15°C to 20°C, corresponding to the crystallization of the PCM, can be noticed, and its intensity increases with the PCM amount. As it could be expected, the melting/crystallization enthalpy values increase with the PCM amount, and the PE_ < 63s_130_p foam shows a ΔH_{m1} value of 50 J/g. However, taking into account the PCM weight concentration within the foams, reported in Table 2, it is possible to see that ΔH_{m1}, ΔH_c, and ΔH_{m2} values are systematically lower than the expected ones. Consequently, the effective PCM contents (PCM_{m1}^{eff}, PCM_c^{eff}, PCM_{m2}^{eff}) are considerably lower than the nominal values reported in Table 2. For instance, the sample PE_ < 63s_130_p has a PCM_{m1}^{eff} value of 33% (instead of 56%) and the sample PE_ < 63s_25_p a value of 1.6% (instead of 20%). These discrepancies are partly due to the presence of residual salt that reduces the effective PCM content and also due to the PCM loss during the production process of samples. Considering that TGA tests highlighted that the differences between the real and the theoretical PCM contents within the samples are relatively small, the discrepancy detected in DSC tests can be also attributed to the breakage of some capsules during the preparation stage. In other words, the paraffin that flew out of the capsules is not able to melt/crystallize within the PE matrix in an efficient way.
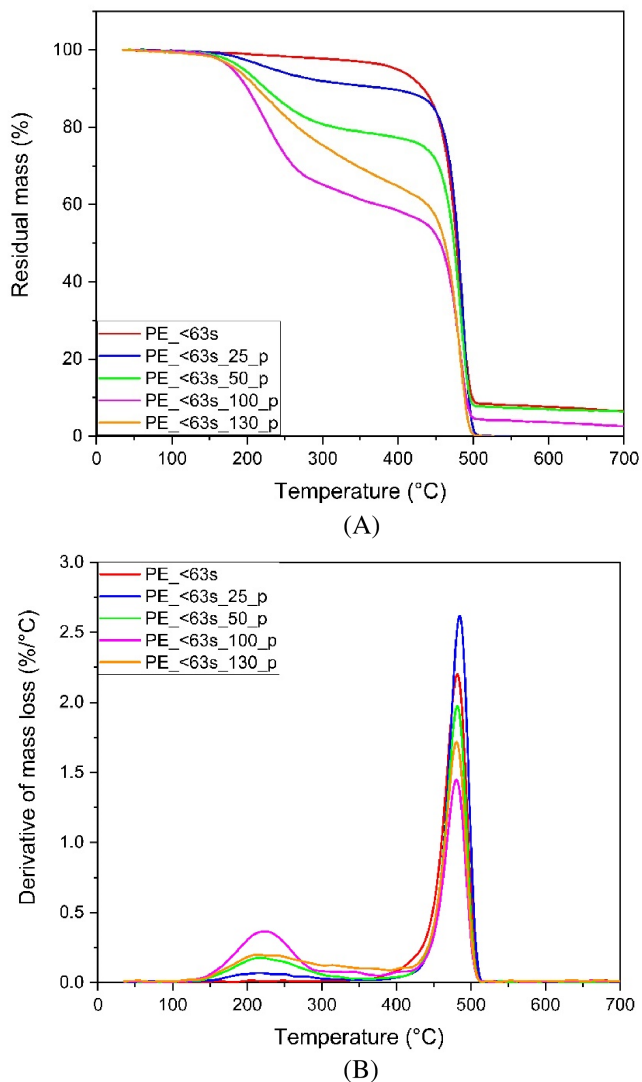

FIGURE 4 Residual mass (A) and derivative of mass loss (B) from TGA tests on the prepared samples

TABLE 6 Results of the TGA tests on the prepared foams

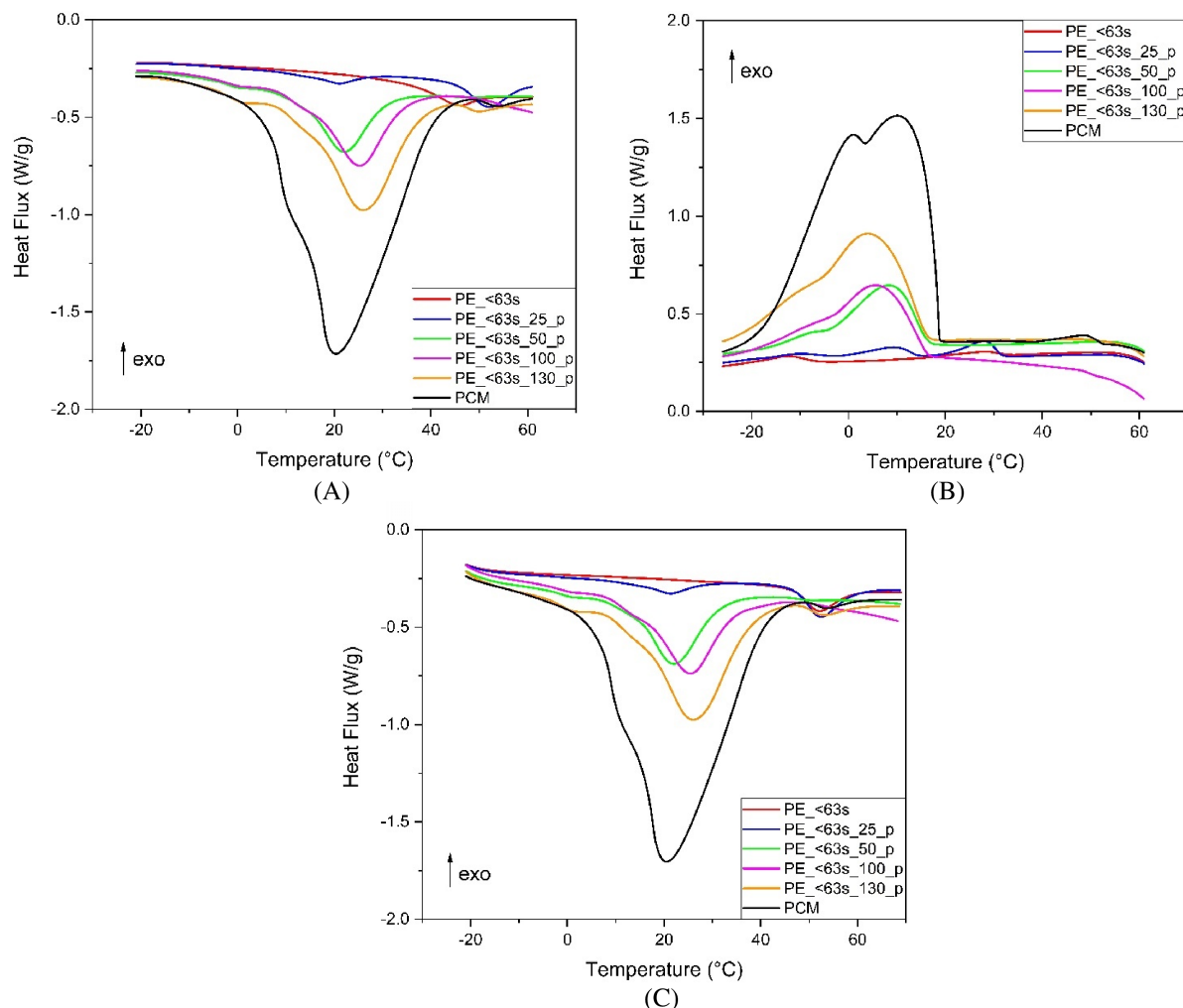| Sample	$T_{5\%}$ (°C)	T_{peak1} (°C)	T_{peak2} (°C)	m_{400} (%)
PE_ < 63s	398.3	-	482.0	-
PE_ < 63s_25_p	234.5	220.7	485.3	89.6
PE_ < 63s_50_p	195.2	219.3	482.2	77.3
PE_ < 63s_100_p	180.5	223.5	480.8	59.4
PE_ < 63s_130_p	185.6	215.0	481.2	64.7

FIGURE 5 Differential scanning calorimetry (DSC) thermograms of the prepared foams and of the neat phase-change material (PCM): (A) first heating, (B) cooling, and (C) second heating scan

TABLE 7 Results of DSC tests on the prepared foams and on the neat PCM

Sample	T_{m1} (°C)	ΔH_{m1} (J/g)	PCM_{m1}^{eff} (%)	T_c (°C)	ΔH_c (J/g)	PCM_c^{eff} (%)	T_{m2} (°C)	ΔH_{m2} (J/g)	PCM_{m2}^{eff} (%)
PE_ < 63s_25_p	22.0	2.5	1.6	9.2	2.0	1.3	21.3	3.2	2.1
PE_ < 63s_50_p	21.9	20.4	13.4	8.6	19.7	12.9	22.0	20.9	13.5
PE_ < 63s_100_p	25.1	31.9	21.0	6.1	33.2	21.7	25.5	34.2	22.0
PE_ < 63s_130_p	25.1	50.6	33.2	4.4	51.2	33.4	26.0	51.5	33.1
PCM	20.3	152.1	-	10.6	153.2	-	20.4	155.4	-

Abbreviations: DSC, differential scanning calorimetry; PCM, phase-change material.

The melting temperature of PCM (T_{m1} and T_{m2}) slightly increases with the PCM amount. On the other hand, the crystallization temperature (T_c) decreases as the PCM content increases. This trend is not due to an intrinsic property of the material, but rather than to the lower thermal conductivity of the foams with respect to the neat PCM. In these conditions, all the thermal

transition are shifted toward higher temperature in the heating scan and to lower temperature in the cooling stage. A similar behavior was also observed for PCM microcapsules dispersed in an acrylic matrix reinforced with carbon fibers, that showed lower crystallization temperature with respect to neat PCM microcapsules.[64] The melting enthalpy values in the first and second heating

ramps (ΔH_{m1} and ΔH_{m2}) are quite similar, meaning that the capability of samples to store heat is retained even when the thermal history of the samples is deleted.

Figure 6A–F reports the results of the thermal imaging tests for the PE_ < 63s_130_p sample. In particular, Figure 6A–C shows pictures taken after 0, 3, and 10 min during the heating scan, while Figure 6D–F represents pictures taken after 0, 3, and 10 min during the cooling test. This analysis allows to investigate the evolution of the surface temperature of the foams upon heating/ cooling stages, in order to better evaluate their effective capability to store/release heat. Moreover, through this analysis, it is possible to evaluate the PCM distribution inside the foam, that corresponds to the colder spots during the heating scan and to the hotter spots during the cooling stage. Looking at Figure 6A,B,D,E, the inhomogeneous distribution of PCM within the foams can be clearly identified. The reason for this inhomogeneity can be the elevated salt content that was added during the mixing process, that hinders the homogeneous distribution of the PCM within the PE matrix.

Figure 7A,B reports the temperature profiles obtained during the thermal imaging tests on the prepared foams, while the most significant results are listed in Table 8. Increasing the amount of PCM inside the foam, both heating and cooling curves are delayed along the time scale. Moreover, in samples containing PCM, an isothermal step corresponding to the phase transition of paraffin at a temperature of around 24°C can be clearly observed. The results reported in Table 8 highlight that PE_ < 63s_130_p

foam is characterized by values of t_5 and t_{40}, which are double in comparison to those of the foam without PCM. The results indicate that, even if part of the PCM was lost during the production process (or it is not able to melt/crystallize once inserted in the PE matrix), the prepared foams are able to store/release an interesting amount of thermal energy in the considered temperature interval.

In Table 9, the values of thermal conductivity are reported. The specimen PE_ < 63s, with no PCM inside, has the lowest value of the thermal conductivity since it is characterized by high values of both open and total porosity. Increasing the amount of PCM inside the foam leads to an increase of the thermal conductivity.

3.4 | Mechanical properties

From the stress–strain curves presented in Figure 8 and from the results reported in Table 10, it is possible to notice that foams without PCM possess the highest specific elastic modulus (183 MPa·cm^3/g) and specific strength (4.8 MPa·cm^3/g). The addition of PCM inside the foam leads to a progressive decrease of the specific strength and of the specific elastic modulus. In particular, the specific elastic modulus decreases from 182.7 MPa·cm^3/g down to 57.4 MPa·cm^3/g in the case of PE_ < 63s_130_p sample. This behavior could be explained by the lower stiffness and strength of the microcapsules compared to the neat PE matrix.[65] The same conclusion can be drawn if Shore A values, reported in Table 10, are considered. Shore A value
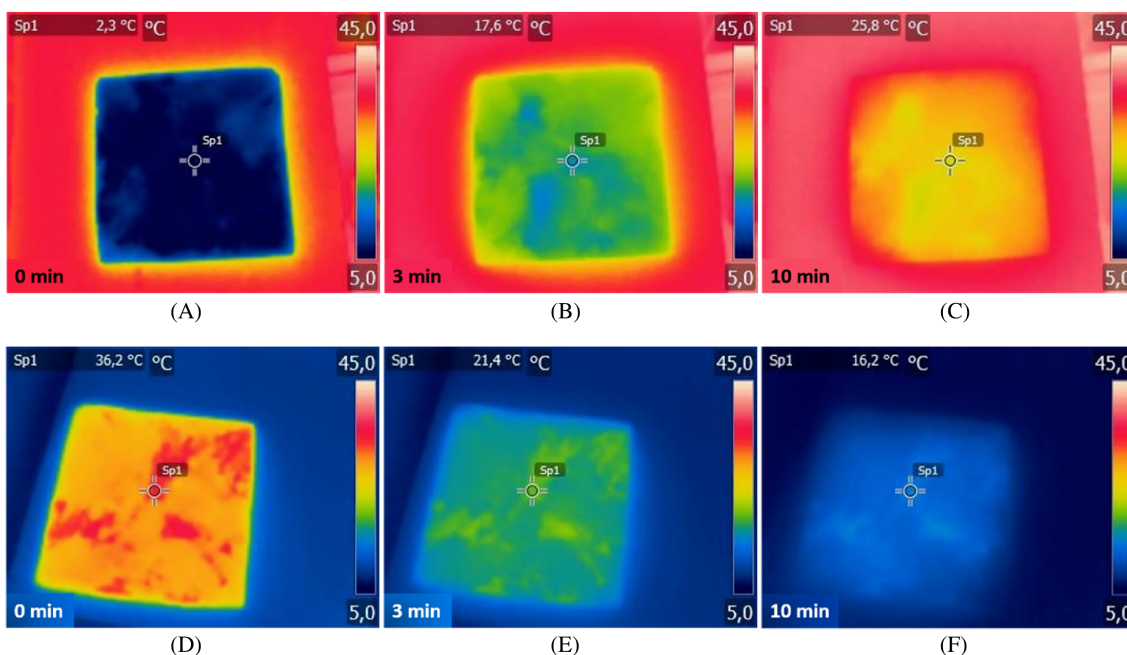

FIGURE 6 IR thermography images after 0, 3, and 10 min of PE_ < 63s_130_p foam during heating (A–C) and cooling (D–E) stages
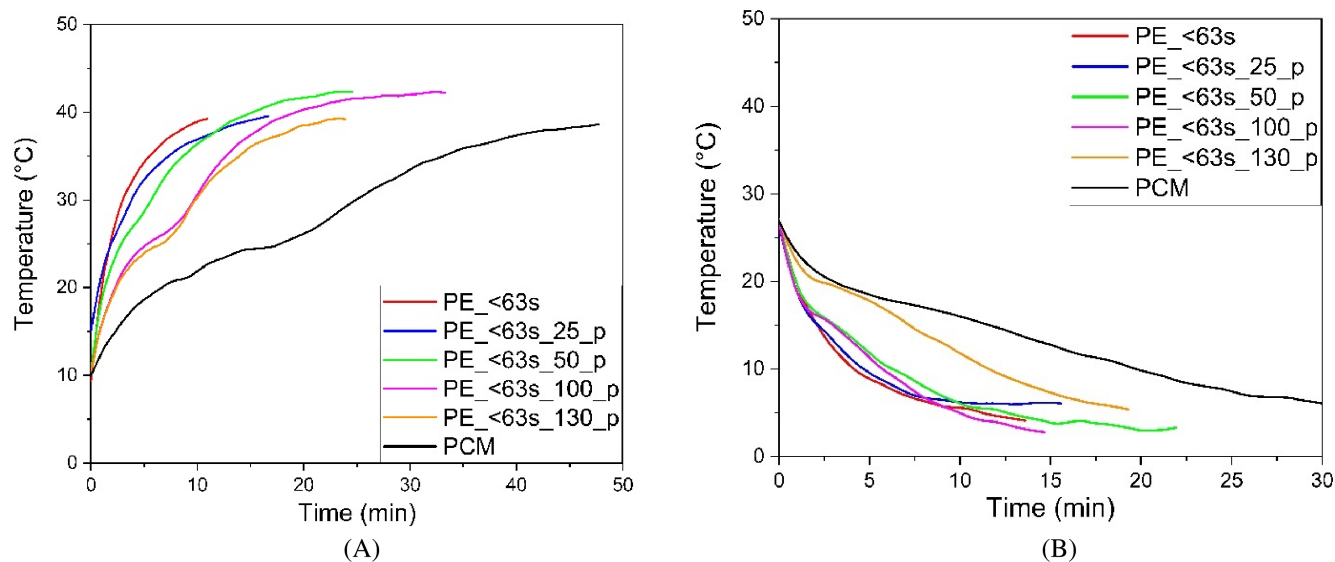
FIGURE 7 Temperature profiles obtained from thermal imaging tests on the prepared foams during (A) heating and (B) cooling stages

TABLE 8 Results of the thermal imaging tests on the prepared foams

Sample	t_{40} (min)	t_5 (min)
PE_ < 63s	10.2 ± 0.5	8.7 ± 0.8
PE_ < 63s_25_p	14.7 ± 0.9	12.7 ± 1.2
PE_ < 63s_50_p	13.6 ± 1.1	10.1 ± 0.6
PE_ < 63s_100_p	18.0 ± 0.7	10.2 ± 1.0
PE_ < 63s_130_p	22.4 ± 1.4	18.5 ± 1.5
PCM	50.2 ± 1.1	30.7 ± 1.0

TABLE 9 Results of the thermal conductivity tests

Sample	Thermal conductivity (W/mK)
PE_ < 63s	0.15 ± 0.01
PE_ < 63s_25_p	0.21 ± 0.01
PE_ < 63s_50_p	0.31 ± 0.02
PE_ < 63s_100_p	0.31 ± 0.05
PE_ < 63s_130_p	0.33 ± 0.03

FIGURE 8 Representative stress–strain curves from quasi-static tensile tests on the prepared foams

for the PE_ < 63s is 80, while it drops down to 67 if the PE_ < 63 s_130p foam is considered.

In a similar way, the specific strength decreases from 4.8 MPa·cm³/g up to 1.9 MPa·cm³/g for the PE_ < 63 s_130p sample. The decreased strength of the foams due to PCM addition can be probably explained by the limited interfacial adhesion between the PE matrix and the PCM microcapsules, as detected in SEM micrographs (see Figure 2F). Interestingly, the strain-at-break values of the foams are considerably increased with the PCM addition, passing from 0.08 mm/min the case of PE_ < 63s
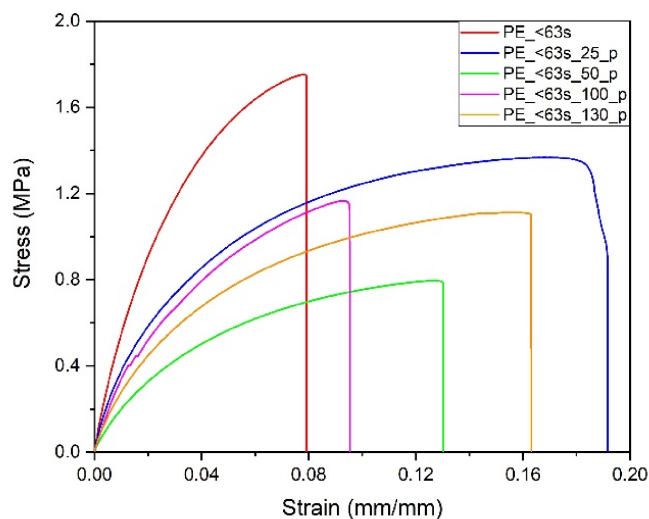
sample up to 0.16 mm/mm for the PE_ < 63s_130_p foam. It can be hypothesized that the observed increase in the strain-at-break values upon PCM addition can be attributed to the toughening mechanism produced by the interfacial debonding between the PE matrix and the microcapsules at elevated deformation levels. In these conditions, a considerable amount of energy must be spent to create debonding surfaces within the samples, with a consequent fracture resistance increase. However, further tests will be required to have a better comprehension of this effect. It is therefore possible to conclude that the addition of paraffin microcapsules within these materials plays a softening effect, with a consistent reduction of the dimensional stability and of the failure resistance, accompanied by an interesting improvement of the ultimate strain levels.

TABLE 10 Results of Shore A hardness and quasi-static tensile tests on the prepared foams

Sample	Shore hardness A	Specific E (MPa·cm³/g)	Specific σ_R (MPa·cm³/g)	ε_R (m/mm)
PE_ < 63s	80 ± 2	182.7 ± 15.6	4.8 ± 0.4	0.08 ± 0.01
PE_ < 63s_25_p	76 ± 4	99.8 ± 24.0	2.5 ± 0.6	0.18 ± .07
PE_ < 63s_50_p	71 ± 8	57.5 ± 18.4	1.6 ± 0.4	0.12 ± 0.02
PE_ < 63s_100_p	76 ± 7	67.7 ± 19.9	1.1 ± 0.5	0.12 ± 0.03
PE_ < 63s_130_p	68 ± 5	57.4 ± 12.1	1.9 ± 0.3	0.16 ± 0.03

4 | CONCLUSIONS

This work demonstrated that the salt leaching technique could be a very interesting method for the sustainable production of polyethylene foams applied in TES applications. Evaluation of water uptake, SEM micrographs, and density measurements allowed to investigate the morphology of the foamed samples, showing that the produced foams were characterized by an open porosity with an interconnected structure and with pore size of about 5–7 μm. The presence of PCM filled part of the pores within the foams, increasing thus their density (from 0.32 g/cm³ in case of neat PE foam up to 0.52 g/cm³ in case of PE_ < 63s_130_p) and reducing water absorption values. Leaking tests performed to evaluate eventual PCM losses highlighted that after 50 heating/cooling cycles the weight loss was lower than 2 wt% for all the prepared samples. Thermogravimetric analysis evidenced that the thermal degradation stability decreased with the PCM amount, but the degradation temperature remained well above the maximum working temperature of these foams in building applications. DSC analysis showed that these materials were able to store/release an interesting amount of thermal energy (up to 50 J/g for PE_ < 63s_130_p foam), even if the measured melting/crystallization enthalpy values were below the theoretical ones. Infrared thermography analysis highlighted that the time required by the PE_ < 63s_130_p sample to reach the set temperatures was doubled with respect to the neat PE foam. The thermal conductivity slightly increased by increasing the PCM content in the foams, from 0.15 W/m·K for PE_ < 63s up to 0.33 W/m·K for PE_ < 63s_130_p. The stiffness, the hardness, and the strength of the foams were considerably reduced upon the PCM addition, probably due to the limited intrinsic mechanical properties of the microcapsules and the low of interfacial adhesion between the PCM and the PE matrix. Interestingly, the strain-at-break values were noticeably improved upon PCM addition. It could be therefore concluded that the prepared foams possessed interesting thermo-mechanical features, and they could be successfully applied for the thermal insulation and the thermal management of buildings. An optimization of the production process should be made in the future to increase the PCM concentration within the foams and to improve the interfacial adhesion between the capsules and the PE matrix.

CONFLICT OF INTEREST
The authors declare that they have no conflict of interest.

DATA AVAILABILITY
The authors declare that the manuscript has no associated data.

ORCID
Alessandro Sorze https://orcid.org/0000-0001-9281-0251
Francesco Valentini https://orcid.org/0000-0001-9496-0501

REFERENCES
[1] S. A. Memon, *Renew. Sustain. Energy Rev.* **2014**, *31*, 870.
[2] N. Soares, J. J. Costa, A. R. Gaspar, P. Santos, *Energy Build* **2013**, *59*, 82.
[3] A. Alexiadis, *Ecol. Modell.* **2007**, *203*(3–4), 243.
[4] S. Hongois, F. Kuznik, P. Stevens, J.-J. Roux, *Sol. Energy Mater. Sol. Cells* **2011**, *95*(7), 1831.
[5] N. R. Jankowski, F. P. McCluskey, *Appl. Energy* **2014**, *113*, 1525.
[6] M. R. Anisur, M. H. Mahfuz, M. A. Kibria, R. Saidur, I. H. S. C. Metselaar, T. M. I. Mahlia, *Renew. Sustain. Energy Rev.* **2013**, *18*, 23.
[7] D. Fernandes, F. Pitié, G. Cáceres, J. Baeyens, *Energy* **2012**, *39*(1), 246.
[8] S. Peng, A. Fuchs, R. A. Wirtz, *J. Appl. Polym. Sci.* **2004**, *93*, 1240.
[9] H. Bo, E. M. Gustafsson, F. Setterwall, *Energy* **1999**, *24*(12), 1015.
[10] A. M. Borreguero, M. Carmona, M. L. Sanchez, J. L. Valverde, J. F. Rodriguez, *Appl. Therm. Eng.* **2010**, *30*(10), 1164.

[11] A. Dorigato, M. V. Ciampolillo, A. Cataldi, M. Bersani, A. Pegoretti, *Rubber Chem. Technol.* **2017**, *90*(3), 575.

[12] Y. E. Milián, A. Gutiérrez, M. Grágeda, S. Ushak, *Renew. Sustain. Energy Rev.* **2017**, *73*, 983.

[13] F. Valentini, A. Dorigato, A. Pegoretti, *Rubber Chem. Technol.* **2021**, *94*(3), 432.

[14] K. Pielichowska, K. Pielichowski, *Prog. Mater. Sci.* **2014**, *65*, 67.

[15] G. Fredi, A. Dorigato, L. Fambri, A. Pegoretti, *Polymer* **2017**, *9*(9), 405.

[16] A. de Gracia, L. F. Cabeza, *Energy Build* **2015**, *103*, 414.

[17] Y. Yuan, N. Zhang, W. Tao, X. Cao, Y. He, *Renew. Sustain Energy Rev* **2014**, *29*, 482.

[18] A. Dorigato, G. Fredi, A. Pegoretti, *Front. Mater.* **2019**, *6*, 76.

[19] F. Valentini, F. Morandini, M. Bergamo, A. Dorigato, *J. Appl. Phys.* **2020**, *128*(7), 075103.

[20] M. M. Farid, A. M. Khudhair, S. A. Razack, S. Al-Hallaj, *Energy Convers. Manage.* **2004**, *45*(9–10), 1597.

[21] C. Castellon, M. Medrano, J. Roca, L. F. Cabeza, M. E. Navarro, A. I. Fernandez, A. Lazaro, B. Zalba, *Renew. Energy* **2010**, *35*(10), 2370.

[22] D. Rigotti, A. Dorigato, A. Pegoretti, *Mater. Today Commun.* **2018**, *15*, 228.

[23] E. Fallahi, M. Barmar, M. H. Kish, *Iranian Polym. J.* **2010**, *19*(4), 277.

[24] F. Salaün, E. Devaux, S. Bourbigot, P. Rumeau, *Thermochim. Acta* **2010**, *506*, 82.

[25] G. Fredi, A. Dorigato, A. Pegoretti, *eXPRESS Polym. Lett.* **2018**, *12*(4), 349.

[26] H. Bo, V. Martin, F. Setterwall, *Energy* **2004**, *29*(11), 1785.

[27] A. Sharma, V. V. Tyagi, C. R. Chen, D. Buddhi, *Renew. Sustain. Energy Rev.* **2009**, *13*(2), 318.

[28] G. Fredi, S. Dirè, E. Callone, R. Ceccato, F. Mondadori, A. Pegoretti, *Materials* **2019**, *12*(8), 1286.

[29] A. F. Regin, S. C. Solanki, J. S. Saini, *Renew. Sustain. Energy Rev.* **2008**, *12*(9), 2438.

[30] S. Phadungphatthanakoon, S. Poompradub, S. P. Wanichwecharungruang, *Appl. Mater. Interfaces* **2011**, *3*(9), 3691.

[31] A. Dorigato, P. Canclini, S. H. Unterberger, A. Pegoretti, *eXPRESS Polymer Letters* **2017**, *11*(9), 738.

[32] Y. Hong, G. Xin-shi, *Sol. Energy Mater. Sol. Cells* **2000**, *64*(1), 37.

[33] I. Krupa, G. Mikova, A. S. Luyt, *Eur. Polym. J.* **2007**, *43*(3), 895.

[34] A. Sari, C. Alkan, A. Karaipekli, O. Uzun, *J. Appl. Polym. Sci.* **2009**, *116*(2), 929.

[35] Q. Cao, L. Pengsheng, *Eur. Polym. J.* **2006**, *42*(11), 2931.

[36] K. Kaygusuz, C. Alkan, A. Sari, O. Uzun, *Energ. Sources, Part A* **2008**, *30*(11), 1050.

[37] K. O. Lee, M. A. Medina, X. Sun, X. Jin, *Solar Energy* **2018**, *163*, 113.

[38] N. Hanchi, H. Hamza, J. Lahjomri, A. Oubarra, International conference on materials and energy 2015 and the international conference on materials and energy 2016, **2017**.

[39] S.-M. Wang, P. Matiašovský, P. Mihálka, C.-M. Lai, *Energ. Build.* **2018**, *159*, 419.

[40] A. Mohebbi, A. Ajji, F. Mighri, D. Rodrigue, *Cell. Polym.* **2015**, *34*, 6.

[41] D. Eaves, *Handbook of Polymer Foams*, Rapra Technology Ldt, Shawbury, UK **2004**.

[42] N. Mills, *Polymer Foams Handbook: Engineering and Biomechanics Applications and Design Guide*, Butterworth-Heinemann, Oxford, UK **2007**.

[43] M. A. Rodriguez-Perez, J. I. Velasco, D. Arencon, O. Almanza, J. A. De Saja, *J. Appl. Polym. Sci.* **2000**, *75*, 156.

[44] J. Stehr, *Gummi Fasern Kunststoffe* **2015**, *68*(12), 821.

[45] W. Michaeli, S. Sitz, *Cell. Polym.* **2010**, *29*(4), 227.

[46] C. Hopmann, F. Lemke, Q. Nguyen Binh, *J. Appl. Polym. Sci.* **2016**, *133*(27), 1.

[47] C. D. Han, C. A. Villamizar, *Polym. Eng. Sci.* **1978**, *18*(9), 687.

[48] D. Kropp, W. Michaeli, T. Herrmann, O. Schröder, *J. Cell. Plast.* **1998**, *34*(4), 304.

[49] R. Gendron, M. F. Champagne, Y. Delaviz, M. E. Polasky, *J. Cell. Plast.* **2006**, *42*(2), 127.

[50] S. H. Oh, S. G. Kang, E. S. Kim, S. H. Cho, J. H. Lee, *Biomaterials* **2003**, *24*, 4011.

[51] R. Scaffaro, F. Lopresti, L. Botta, S. Rigogliuso, G. Ghersi, *Macromol. Mater. Eng.* **2016**, *301*(2), 182.

[52] R. Scaffaro, F. Lopresti, L. Botta, S. Rigogliuso, G. Ghersi, *J. Mech. Behav. Biomed. Mater.* **2016**, *54*, 8.

[53] S. G. Mosanenzadeh, H. E. Naguib, C. B. Park, N. Atalla, *Polym. Eng. Sci.* **2013**, *53*(9), 1979.

[54] R. Scaffaro, F. Lopresti, L. Botta, S. Rigogliuso, G. Ghersi, *J. Mech. Behav. Biomed. Mater.* **2016**, *63*, 303.

[55] R. Kroon, J. D. Ryan, D. Kiefer, L. Yu, J. Hynynen, E. Olsson, C. Müller, *Adv. Funct. Mater.* **2017**, *27*(47), 1704183.

[56] W. Trakanpruk, Y. Rodthong, *J. Metals, Mater. Miner.* **2008**, *18*(2), 33.

[57] E. Zonta, F. Valentini, A. Dorigato, L. Fambri, A. Pegoretti, *Polym. Eng. Sci.* **2021**, *61*(1), 136.

[58] F. Valentini, L. Fambri, A. Dorigato, A. Pegoretti, *Front. Mater.* **2021**, *8*, 101.

[59] Q. Chen, J. Zhao, J. Ren, L. Rong, P. F. Cao, R. C. Advincula, *Adv. Funct. Mater.* **2019**, *29*(23), 1900469.

[60] Q. Hou, D. W. Grijpma, J. Feijen, *Biomaterials* **2003**, *24*(11), 1937.

[61] R. Scaffaro, F. Lopresti, L. Botta, A. Maio, *Compos. Part B* **2016**, *98*, 70.

[62] A. Chilali, M. Assarar, W. Zouari, H. Kebir, R. Ayad, *Compos. - A: Appl. Sci. Manuf.* **2017**, *95*, 75.

[63] F. X. Alvarez, D. Jou, A. Sellitto, *Appl. Phys. Lett.* **2010**, *97*, 3.

[64] G. Fredi, A. Dorigato, A. Pegoretti, *Polym. Compos.* **2019**, *40*(9), 3711.

[65] G. Fredi, A. Dorigato, L. Fambri, A. Pegoretti, *Polym. Eng. Sci.* **2020**, *60*(6), 1202.